



**Direct Measurement of Molecular Mobility in Actively Deformed Polymer Glasses**

Hau-Nan Lee, *et al.*  
*Science* **323**, 231 (2009);  
DOI: 10.1126/science.1165995

**The following resources related to this article are available online at [www.sciencemag.org](http://www.sciencemag.org) (this information is current as of January 8, 2009 ):**

**Updated information and services**, including high-resolution figures, can be found in the online version of this article at:

<http://www.sciencemag.org/cgi/content/full/323/5911/231>

**Supporting Online Material** can be found at:

<http://www.sciencemag.org/cgi/content/full/1165995/DC1>

This article **cites 28 articles**, 2 of which can be accessed for free:

<http://www.sciencemag.org/cgi/content/full/323/5911/231#otherarticles>

This article appears in the following **subject collections**:

Materials Science

[http://www.sciencemag.org/cgi/collection/mat\\_sci](http://www.sciencemag.org/cgi/collection/mat_sci)

Information about obtaining **reprints** of this article or about obtaining **permission to reproduce this article** in whole or in part can be found at:

<http://www.sciencemag.org/about/permissions.dtl>

spectral function can be written as a convolution of contributions from the left and right branches. Universal function  $A(\epsilon)$  in Eq. 1 is related to  $D(y)$  as

$$A(\epsilon) = \int_{-1}^1 dy D(y) \theta(\epsilon - y) (\epsilon - y)^{\frac{\delta_{\pm}}{2\pi} - 1} \quad (11)$$

One can analytically obtain limiting behavior of  $D(y)$  for  $y \rightarrow \pm 1$  from Eqs. 9 to 11 as  $D(y) \propto (1 \mp y)^{d_{\pm}}$  for  $y \rightarrow \pm 1$ , where

$$d_{+} = \left(\frac{\delta_{+}}{2\pi}\right)^2 - 1, \quad d_{-} = \left(2 - \frac{\delta_{+}}{2\pi}\right)^2 - 1 > 3 \quad (12)$$

At moderate interaction strength,  $\overline{\mu_{0,+}} > 0$ , function  $A(\epsilon)$  diverges at  $\epsilon = 1$ . Then the ratio of the prefactors above and below the singular line is universal,

$$\lim_{|\delta\epsilon| \rightarrow 0} \frac{A(1 + |\delta\epsilon|)}{A(1 - |\delta\epsilon|)} = \frac{\Gamma\left[\frac{\delta_{+}}{2\pi}\right]^2 \Gamma\left[1 - \left(\frac{\delta_{+}}{2\pi}\right)^2\right]}{\Gamma\left[\frac{\delta_{-}}{2\pi}\right]^2 \Gamma\left[1 - \left(\frac{\delta_{-}}{2\pi}\right)^2\right]} \quad (13)$$

To evaluate  $D(y)$  away from the edges, one should be able to calculate the dynamics of chiral vertex operators (11). For a nonlinear spectrum, this is a very nontrivial problem, the analytic solution of which is not known. Similar correlators have attracted attention recently (12, 13), and their connection to the nonlinear quantum shock wave dynamics and nonlinear differential equations has been discussed. Although it might be possible to proceed similarly for the evaluation of  $D(y)$ , it is not clear whether nonlinear differential equations obtained this way will have an analytic solution. We use an alternative approach of (14, 15), which allows us to develop a representation of  $D(y)$  in terms of certain determinants built of single-particle (rather than many-body) states. These determinants can be evaluated numerically, which practically solves the problem of finding  $D(y)$ . Representative results for  $D(y)$  and  $A(\epsilon)$  for  $K = 4.54$  are shown in Fig. 3.

The universal Hamiltonian given by Eqs. 2 and 5 can be also used to describe gapless bosonic and spin  $-\frac{1}{2}$  systems away from particle hole symmetric ground states. We present main results on singularities of their dynamic response functions in SOM (11).

We have constructed universal low-energy theory of a wide class of interacting 1D quantum liquids without resorting to the simplifications of the Tomonaga-Luttinger model accepted in the phenomenological LL description. Unlike the latter, we keep the nonlinear dispersion relation of the fermions intact. The replacement of the dispersion relation by a linear one,  $\omega = vp$ , results in an artificial introduction of Lorentz invariance into the system. Although not affecting the low-energy behavior of local properties (such as the local tunneling density of states), the introduced

symmetry alters qualitatively the predictions for the momentum-resolved quantities, such as the spectral function. Keeping the nonlinearity allows us to find the generic low-energy behavior of the dynamic response functions of a system of interacting fermions, bosons, and spins. Possible extensions of our theory should be able to describe the effects of finite temperature, spin systems at particle-hole symmetric points, systems with long-range interactions, and fermions with spin.

#### References and Notes

1. F. D. M. Haldane, *Phys. Rev. Lett.* **47**, 1840 (1981).
2. F. D. M. Haldane, *J. Phys. C* **14**, 2585 (1981).
3. T. Giamarchi, *Quantum Physics in One Dimension* (Oxford Univ. Press, New York, 2004).
4. M. Pustilnik, E. G. Mishchenko, L. I. Glazman, A. V. Andreev, *Phys. Rev. Lett.* **91**, 126805 (2003).
5. O. M. Auslaender *et al.*, *Science* **295**, 825 (2002).
6. S. Tomonaga, *Prog. Theor. Phys.* **5**, 544 (1950).
7. J. M. Luttinger, *J. Math. Phys.* **4**, 1154 (1963).
8. D. C. Mattis, E. H. Lieb, *J. Math. Phys.* **6**, 304 (1965).
9. I. E. Dzyaloshinskii, A. I. Larkin, *Sov. Phys. JETP* **38**, 202 (1974).
10. A. Luther, I. Peschel, *Phys. Rev. B* **9**, 2911 (1974).
11. Materials and methods are available as supporting material on Science Online.
12. E. Bettelheim, A. G. Abanov, P. Wiegmann, *Phys. Rev. Lett.* **97**, 246402 (2006).
13. E. Bettelheim, A. G. Abanov, P. Wiegmann, *J. Phys. A* **41**, 392003 (2008).
14. D. A. Abanin, L. S. Levitov, *Phys. Rev. Lett.* **93**, 126802 (2004).
15. D. A. Abanin, L. S. Levitov, *Phys. Rev. Lett.* **94**, 186803 (2005).
16. L.-M. Duan, *Phys. Rev. Lett.* **96**, 103201 (2006).
17. T.-L. Dao, A. Georges, J. Dalibard, C. Salomon, I. Carusotto, *Phys. Rev. Lett.* **98**, 240402 (2007).
18. S. R. White, *Phys. Rev. Lett.* **69**, 2863 (1992).
19. U. Schollwöck, *Rev. Mod. Phys.* **77**, 259 (2005).
20. R. G. Pereira *et al.*, *Phys. Rev. Lett.* **96**, 257202 (2006).
21. K. Samokhin, *J. Phys.* **10**, L533 (1998).
22. M. Pustilnik, M. Khodas, A. Kamenev, L. I. Glazman, *Phys. Rev. Lett.* **96**, 196405 (2006).
23. M. Khodas, M. Pustilnik, A. Kamenev, L. I. Glazman, *Phys. Rev. B* **76**, 155402 (2007).
24. R. G. Pereira, S. R. White, I. Affleck, *Phys. Rev. Lett.* **100**, 027206 (2008).
25. V. V. Cheianov, M. Pustilnik, *Phys. Rev. Lett.* **100**, 126403 (2008).
26. A. Imambekov, L. I. Glazman, *Phys. Rev. Lett.* **100**, 206805 (2008).
27. A. V. Rozhkov, *Eur. Phys. J. B* **47**, 193 (2005).
28. A. V. Rozhkov, *Phys. Rev. B* **74**, 245123 (2006).
29. A. V. Rozhkov, *Phys. Rev. B* **77**, 125109 (2008).
30. We thank A. Kamenev and D. Abanin for useful discussions. This work was supported by U.S. Department of Energy grant no. DE-FG02-08ER46482.

#### Supporting Online Material

www.sciencemag.org/cgi/content/full/1165403/DC1

Materials and Methods

Fig. S1

Table S1

References

3 September 2008; accepted 10 November 2008

Published online 27 November 2008;

10.1126/science.1165403

Include this information when citing this paper.

## Direct Measurement of Molecular Mobility in Actively Deformed Polymer Glasses

Hau-Nan Lee, Keewook Paeng, Stephen F. Swallen, M. D. Ediger

When sufficient force is applied to a glassy polymer, it begins to deform through movement of the polymer chains. We used an optical photobleaching technique to quantitatively measure changes in molecular mobility during the active deformation of a polymer glass [poly(methyl methacrylate)]. Segmental mobility increases by up to a factor of 1000 during uniaxial tensile creep. Although the Eyring model can describe the increase in mobility at low stress, it fails to describe mobility after flow onset. In this regime, mobility is strongly accelerated and the distribution of relaxation times narrows substantially, indicating a more homogeneous ensemble of local environments. At even larger stresses, in the strain-hardening regime, mobility decreases with increasing stress. Consistent with the view that stress-induced mobility allows plastic flow in polymer glasses, we observed a strong correlation between strain rate and segmental mobility during creep.

Glasses form when molecular motion becomes slow, and thus liquidlike flow in a glass would seem impossible by definition. Nevertheless, polymer glasses under stress can yield and undergo plastic flow (1). In this process, the glass dissipates enormous amounts of energy without breaking. This toughness is

the critical design requirement in many applications, and efforts to understand it go back more than 70 years. In 1936, Eyring (2) proposed a model in which external loading lowers the energy barriers for molecular motion and thus effectively transforms a glass into a viscous liquid. Other workers (1, 3–7) have modified Eyring's approach in important ways while maintaining the central idea that stress can induce molecular mobility.

Department of Chemistry, University of Wisconsin–Madison, Madison, WI 53706, USA.

Recent work on “jamming” systems (amorphous systems that develop a yield stress) suggests the generality of this idea; as in the case of sand piles or colloids, one can unjam polymer glasses by applying stress (8). Mechanical measurements have been used to infer huge increases in molecular mobility in polymer glasses due to stress (9–11), but this interpretation is controversial (12). Nuclear magnetic resonance (13), an optical technique (14), and several simulations (15–18) have directly demonstrated that molecular mobility in polymer glasses is accelerated during deformation. Nevertheless, the absence of quantitative molecular mobility measurements on polymer glasses during deformation limits the development of predictive models of polymer deformation. In the absence of such information, the Eyring model or a related approach is assumed to be valid (1, 4–6).

Here we report optical measurements of stress-induced molecular mobility in a lightly cross-linked poly(methyl methacrylate) (PMMA) glass with a glass transition temperature  $T_g = 395$  K (19). We quantitatively measured changes in polymer segmental mobility with external loading and compared these data to the Eyring model (2). In the low-stress regime, the Eyring model correctly describes changes in the segmental mobility. However, as deformation continues into the flow regime, mobility speeds up by more than a factor of 1000, and the Eyring model fails to capture this behavior. We show that spatially heterogeneous dynamics (20) have a substantial influence on the deformation of polymer glasses in this regime. In addition, we observed a strong correlation between strain rate and mobility, supporting the view that stress-induced mobility allows polymer glasses to flow.

We used a confocal fluorescence microscope system to measure molecular mobility during deformation, as described previously (14). We deformed the PMMA glass uniaxially in tension with a constant external load. During this creep experiment, we used an optical photobleaching technique to measure the reorientation of a dilute molecular probe (*N,N*-dipentyl-3,4,9,10-perylene dicarboximide). The reorientation of this probe is an excellent reporter of the segmental dynamics of PMMA (21) (fig S2). We optically measured strain and mobility in the same small region (~200 by 250  $\mu\text{m}$ ) of the sample.

Mobility changes during one creep experiment on PMMA glass at 375.7 K ( $T_g - 19$  K) are shown in Fig. 1. The strain change during creep with engineering stress equal to 16.0 MPa followed by recovery at 0.7 MPa are shown in Fig. 1A. Strain ( $\epsilon$ ) is defined as  $\epsilon(t) = [L(t) - L_0]/L_0$ , where  $L_0$  is the initial distance (~200  $\mu\text{m}$ ) between two lines photobleached in the sample and  $L(t)$  is the distance at time  $t$ . We observed homogeneous deformation up to  $\epsilon = 0.15$ , after which necking occurred. Initially, the strain rate continuously increased as the sample flowed. After 5000 s, the strain rate decreased, which indicated that strain-hardening was occurring

(22, 23). Creep experiments at lower stresses additionally exhibited an initial regime in which the strain rate decreased before increasing; we define flow onset as this minimum in the local strain rate.

During creep and recovery, we performed ~35 photobleaching experiments to determine

the mobility of PMMA. The anisotropy decay function  $r(t)$ , measured with a polarized photobleaching technique, describes probe reorientation with time. Some anisotropy decays are shown in Fig. 1B. As the strain and strain rates increased, we observed faster  $r(t)$  decays (curve a to curve e), indicating higher mobility. In the

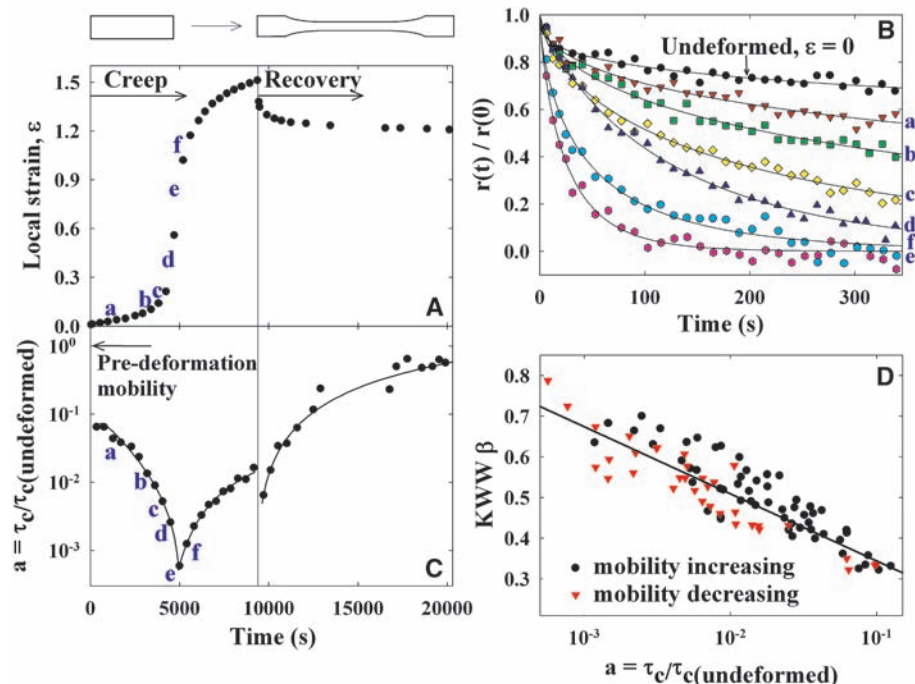
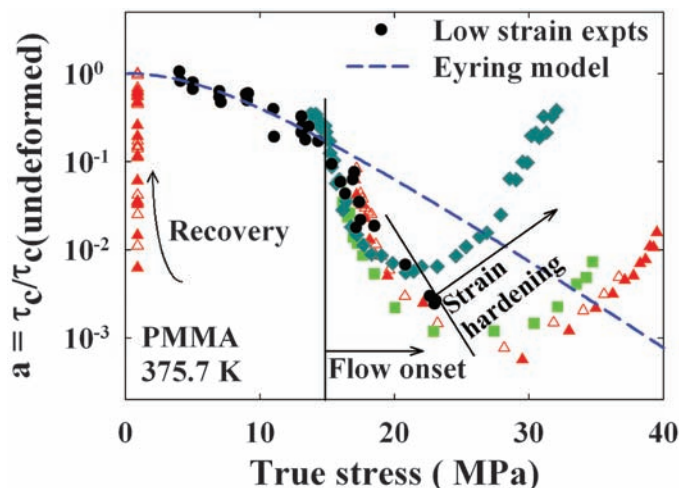


**Fig. 1.** Simultaneous local measurements of strain and mobility in PMMA glass. (A) Strain during creep experiments at 375.7 K with an engineering stress of 16.0 MPa, followed by recovery. The initial and final shapes of the sample are shown. (B) Normalized anisotropy decays obtained during the creep experiment at times indicated by letters a to f. As the strain rate increased, higher mobility (faster anisotropy decay) was observed. The solid lines are KWW fits to the data. (C) Mobility shift factor during creep and recovery. Mobility increased by up to a factor of 1000. The solid lines are guides to the eye. (D) Correlation between the KWW  $\beta$  parameter and mobility for three different trials with stresses in the range of 15.5 to 16.0 MPa. Data were acquired as the mobility was both increasing ( $\bullet$ ) and decreasing ( $\blacktriangledown$ ). The solid line is a fit to the data.

**Fig. 2.** Molecular mobility as a function of the true stress for PMMA at 375.7 K. Solid circles indicate low-strain experiments. The symbols  $\blacktriangle$ ,  $\blacktriangle$ ,  $\blacksquare$ , and  $\blacklozenge$  represent measurements at higher strains with engineering stresses of 16.0, 16.0, 15.5, and 13.5 MPa, respectively; the true stress increased as the strain increased because the cross-sectional area decreased as the sample elongated. Duplicate measurements with an engineering stress of 16 MPa are shown as an indication of reproducibility; mobilities during recovery for these two experiments are shown on the left side. The dashed line shows a fit to the Eyring model.



strain-hardening regime, the strain rate decreases, and  $r(t)$  decays more slowly (curve e to curve f).

To quantitatively analyze mobility changes during creep and recovery, we fit the anisotropy decay to the Kohlrausch-Williams-Watts (KWW) equation  $r(t) = r(0)\exp[-(t/\tau)^\beta]$ , where  $\beta$  determines the nonexponentiality of the decay and  $\tau$  is the rotational relaxation time. The integral of  $r(t)/r(0)$  provides the rotational correlation time  $\tau_c$ , and we define the mobility shift factor  $a = \tau_{c,deformed}/\tau_{c,undeformed}$ .

The changes in mobility during creep and recovery are shown in Fig. 1C. Immediately after the stress was applied, the mobility increased by a factor of 10 and then further increased until dynamics were accelerated 1000-fold relative to the undeformed glass. In the strain-hardening regime, the mobility decreased as the strain rate decreased, even though the strain and true stress increased. After the stress was removed, the mobility first increased and then decreased toward the mobility of the undeformed PMMA.

To compare our results with theoretical models, we plot the segmental mobility as a function of true stress in Fig. 2; two different types of experiments are shown. For low-strain experiments, we performed a single mobility measurement immediately after applying the stress. In these experiments, the deformations are homogenous, and the strains are generally very small ( $\epsilon \ll 0.1$ ). Results are also presented for experiments such as the one illustrated in Fig. 1; here, multiple mobility measurements were performed during one creep experiment, and the overall strain was large ( $\epsilon \sim 1.4$ ).

Three different regimes are illustrated in Fig. 2. In the low-stress regime ( $<15$  MPa), the Eyring model can describe the data. The Eyring model predicts that the response of the segmental relaxation time  $\tau$  of a polymer glass to an applied stress  $\sigma$  is  $\tau \propto \sigma / \sinh(\frac{\sigma \cdot V}{2 \cdot k_B T})$ , where  $k_B$  is the Boltzmann constant,  $T$  is the temperature, and  $V$  is the activation volume. Fitting the low-stress data to the Eyring model yields  $V = 2.7 \text{ nm}^3$ ,

which can be interpreted as indicating the cooperative movement of two to three statistical (or Kuhn) segments. This activation volume is qualitatively consistent with the size of shear transformation zones (24) for colloidal glasses as determined by visualizing microscopic strain during shear; the reported activation volume is about four particle volumes (25). The data in the low-stress regime are also consistent with the predictions of Chen and Schweizer (7), who incorporate ideas from Eyring's treatment into a microscopic model of cage escape.

Figure 2 shows a very large mobility enhancement with the onset of flow ( $\sigma > 15$  MPa), and the Eyring model fails to capture this behavior. In this regime, in addition to lowering the barriers for molecular motion, deformation apparently modifies spatially heterogeneous dynamics in the glass. Molecular motions in supercooled liquids and glasses are spatially heterogeneous (20, 26), and the KWW  $\beta$  parameter provides an indication of the distribution of relaxation times (20). In the low-stress regime,  $\beta$  was unaltered from that of the undeformed sample ( $\beta = 0.32$ ). As mobility increased in the flow regime, the anisotropy decay function became more exponential ( $\beta \rightarrow 1$ ) (Fig. 1D). This result indicates a narrowing of the distribution of relaxation times that reflects the dynamics in slow regions accelerating more than in mobile regions. We speculate that stress is concentrated in slow regions during flow.

At the largest stresses shown in Fig. 2, the mobility decreased with increasing stress in a manner that depended upon the deformation history of particular samples. All of the samples shown were in the strain-hardening regime with strains greater than  $\sim 0.7$ . Such large strains orient the polymer chains (27), and the resulting structure effectively resists deformation (23). The Eyring model does not incorporate polymer structure and qualitatively predicts the wrong trend in this regime.

Consistent with earlier experiments (13) and simulations (15, 17, 18), we emphasize that mo-

lecular mobility in polymer glasses depends on more than the instantaneous true stress. In contrast to Eyring's prediction, the recovery data in Figs. 1 and 2 show a wide range of mobilities even though the stress is constant at a very low value. Although true stress is an important parameter for determining the mobility of polymer glasses, variables such as strain and strain rate can also play an important role.

The connection between molecular motion and macroscopic mechanical properties is illustrated in Fig. 3, in which we plot the dimensionless strain rate as a function of instantaneous molecular mobility. An excellent master curve is obtained for experiments at three temperatures. Also shown in Fig. 3 are predictions from a microscopic theory of mobility in PMMA (28) and the result of computer simulations of a coarse-

**Fig. 3.** Dimensionless strain rate as a function of molecular mobility, illustrating that stress-induced mobility allows polymer flow. The solid line is a fit to the data. The long-dashed line is the model prediction from (28) and the short-dashed line is the molecular dynamics simulation from (18).

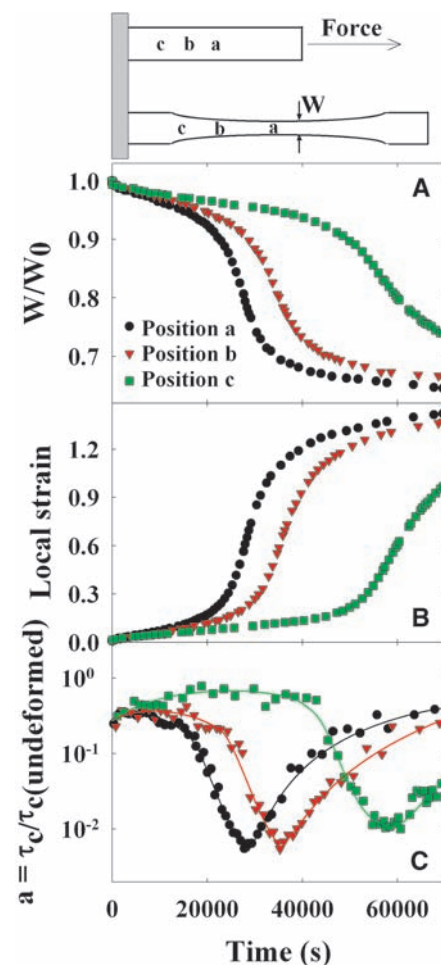
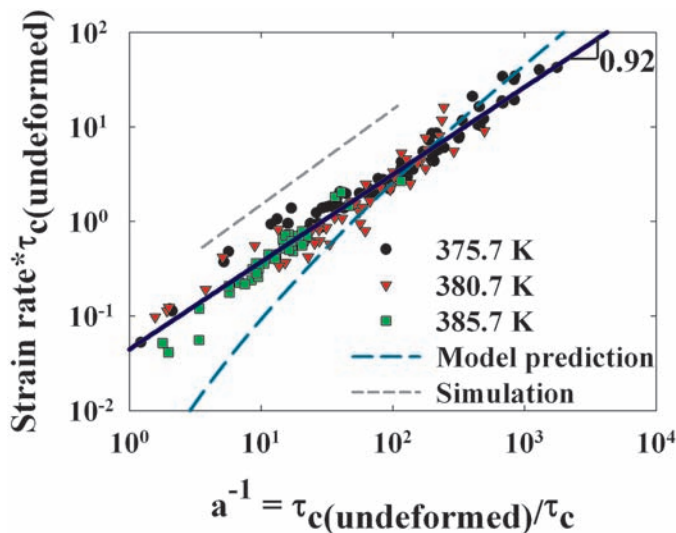


**Fig. 4.** Simultaneous strain and mobility measurements in three different positions of an inhomogeneously deformed PMMA glass at 375.7 K. Panels show the time evolution of the sample width (A), the local strain (B), and the mobility (C). The engineering stress is 13.5 MPa, the initial width ( $W_0$ ) is 2.3 mm ( $W$ , final width). The picture on the top illustrates positions a, b, and c before and after the deformation. Before the deformation, positions b and c were 1.5 and 2.7 mm away from position a, respectively. The solid lines are guides to the eye.

grained polymer glass (18). Our results confirm that stress-induced mobility allows polymer glasses to flow; a 1000-fold increase in mobility very nearly resulted in a 1000-fold increase in the flow rate. These results also strongly support the reliability of probe reorientation as an indicator of polymer mobility during deformation. Figure 3 only includes data from single-step creep experiments; data from recovery and multistep creep experiments do not fall on the same curve. This finding suggests that no mechanical variable universally exhibits a simple relation with molecular mobility.

Because we measured the strain and segmental mobility locally, we were able to perform simultaneous measurements in different parts of an inhomogeneously deformed sample. Mobility changes in three different positions of a sample that necked during deformation are shown in Fig. 4. Plots of sample width and local strain versus time are shown in Fig. 4, A and B, and illustrate necking that begins at position a and then propagates toward positions b and c. Changes in mobility at positions a, b, and c are shown in Fig. 4C. At each position, mobility accelerates as the local strain rate increases; data from all three positions are quantitatively consistent with the master curve in Fig. 3. In a necked sample, molecular mobility is fastest in the shoulder, rather than the neck, even though the true stress in the neck is greater than any other region in the sample.

Polymer glasses are nonequilibrium thermodynamic systems, and we briefly discuss how this influences the interpretation of our measurements. Physical aging describes the change in mechanical properties that occurs over time because of the very slow molecular rearrangements in a glass (11); molecular motions have been shown to slow during physical aging (29). Mechanical experiments on polymer glasses have sometimes been interpreted as a reversal of physical aging, or “rejuvenation” (1, 9–12). We attribute the changes in mobility in our experiment to the combination of deformation-induced mobility and physical aging/rejuvenation. It appears that deformation-induced mobility is the much greater effect in these experiments. For example, the green curve in Fig. 4C shows a small mobility decrease in the first 30,000 s, which we attribute to physical aging. This mobility decrease is similar in magnitude to the decrease caused by physical aging in the undeformed sample during the same time period.

Concepts from the jamming field might be useful for describing the behavior of polymer glasses under stress (8). According to this view, one can unjam glasses either by raising the temperature or applying stress (8, 18, 30). In our experiments, temperature and stress had a qualitatively different effect on molecular mobility. A 1000-fold increase in mobility by deformation at constant temperature changed the KWW  $\beta$  to about 0.8 (Fig. 1D). In the absence of deformation, a 1000-fold increase in mobility occurred

when the temperature was increased by 18 K, but at this temperature  $\beta$  was unchanged at 0.32. Thus, stress not only increased mobility but also, in contrast to temperature, sharpened the distribution of relaxation times. In the low-stress regime in Fig. 2, temperature and stress both increased mobility without narrowing the distribution of relaxation times.

Our results quantify mobility changes in an actively deformed polymer glass and establish a quantitative connection between molecular mobility and macroscopic deformation. We find that mobility is not a function of instantaneous stress alone but can also depend on strain and the deformation history. Plastic flow appears to modify spatially heterogeneous dynamics in the glass, which suggests that there is a complex interplay between microscopic motions and flow. We anticipate that quantitative measurements of molecular mobility during deformation, coupled with appropriate microscopic theory, will lead to substantially improved predictions of the nonlinear deformation behavior of polymer glasses.

#### References and Notes

- H. E. H. Meijer, L. E. Govaert, *Prog. Polym. Sci.* **30**, 915 (2005).
- H. Eyring, *J. Chem. Phys.* **4**, 283 (1936).
- R. E. Robertson, *J. Chem. Phys.* **44**, 3950 (1966).
- M. C. Boyce, D. M. Parks, A. S. Argon, *Mech. Mater.* **7**, 15 (1988).
- C. P. Buckley, D. C. Jones, *Polymer* **36**, 3301 (1995).
- J. M. Caruthers, D. B. Adolf, R. S. Chambers, P. Shrikhande, *Polymer* **45**, 4577 (2004).
- K. Chen, K. S. Schweizer, *Europhys. Lett.* **79**, 26006 (2007).
- A. J. Liu, S. R. Nagel, *Nature* **396**, 21 (1998).
- A. F. Yee, R. J. Bankert, K. L. Ngai, R. W. Rendell, *J. Polym. Sci. Part Polym. Phys.* **26**, 2463 (1988).
- J. J. Martinez-Vega, H. Trumel, J. L. Gacounolle, *Polymer* **43**, 4979 (2002).

- L. C. E. Struik, *Physical Aging in Amorphous Polymers and Other Materials* (Elsevier, New York, 1978).
- G. B. McKenna, *J. Phys. Condens. Matter* **15**, 5737 (2003).
- L. S. Loo, R. E. Cohen, K. K. Gleason, *Science* **288**, 116 (2000).
- H.-N. Lee, K. Paeng, S. F. Swallen, M. D. Ediger, *J. Chem. Phys.* **128**, 134902 (2008).
- F. M. Capaldi, M. C. Boyce, G. C. Rutledge, *Phys. Rev. Lett.* **89**, 175505 (2002).
- A. V. Lyulin, B. Vorselaars, M. A. Mazo, N. K. Balabaev, M. A. J. Michels, *Europhys. Lett.* **71**, 618 (2005).
- R. A. Riggelman, H.-N. Lee, M. D. Ediger, J. J. de Pablo, *Phys. Rev. Lett.* **99**, 215501 (2007).
- R. A. Riggelman, K. S. Schweizer, J. J. de Pablo, *Macromolecules* **41**, 4969 (2008).
- Materials and methods are available as supporting material on Science Online.
- M. D. Ediger, *Annu. Rev. Phys. Chem.* **51**, 99 (2000).
- R. Bergman, F. Alvarez, A. Alegria, J. Colmenero, *J. Non-Cryst. Solids* **235**, 580 (1998).
- H. G. H. van Melick, L. E. Govaert, H. E. H. Meijer, *Polymer* **44**, 2493 (2003).
- E. J. Kramer, *J. Polym. Sci. Part B Polym. Phys.* **43**, 3369 (2005).
- M. L. Falk, J. S. Langer, *Phys. Rev. E* **57**, 7192 (1998).
- P. Schall, D. A. Weitz, F. Spaepen, *Science* **318**, 1895 (2007).
- E. R. Weeks, J. C. Crocker, A. C. Levitt, A. Schofield, D. A. Weitz, *Science* **287**, 627 (2000).
- F. Casas, C. Alba-Simionesco, H. Montes, F. Lequeux, *Macromolecules* **41**, 860 (2008).
- K. Chen, K. S. Schweizer, *Macromolecules* **41**, 5908 (2008).
- C. T. Thureau, M. D. Ediger, *J. Chem. Phys.* **116**, 9089 (2002).
- T. K. Haxton, A. J. Liu, *Phys. Rev. Lett.* **99**, 195701 (2007).
- This work was supported by NSF through grant NIRT-0506840. We thank K. Schweizer, J. Caruthers, G. Medvedev, J. de Pablo, and R. Riggelman for helpful discussions.

#### Supporting Online Material

www.sciencemag.org/cgi/content/full/1165995/DC1

Materials and Methods

Figs. S1 to S3

References

16 September 2008; accepted 18 November 2008  
10.1126/science.1165995

## Suppression of Metallic Conductivity of Single-Walled Carbon Nanotubes by Cycloaddition Reactions

Mandakini Kanungo,<sup>1</sup> Helen Lu,<sup>2</sup> George G. Malliaras,<sup>1</sup> Graciela B. Blanchet<sup>2\*</sup>

The high carrier mobility of films of semiconducting single-walled carbon nanotubes (SWNTs) is attractive for electronics applications, but the presence of metallic SWNTs leads to high off-currents in transistor applications. The method presented here, cycloaddition of fluorinated olefins, represents an effective approach toward converting the “as grown” commercial SWNT mats into high-mobility semiconducting tubes with high yield and without further need for carbon nanotube separation. Thin-film transistors, fabricated from percolating arrays of functionalized carbon nanotubes, exhibit mobilities >100 square centimeters per volt-second and on-off ratios of 100,000. This method should allow for the use of semiconducting carbon nanotubes in commercial electronic devices and provide a low-cost route to the fabrication of electronic inks.

Single-walled carbon nanotubes (SWNTs) are potential candidates for application in electronic devices (1–4). The most severe drawback in this effort has been that the as-synthesized SWNTs are a mixture of semi-

conducting (SC) and metallic (M) tubes, hindering their application in thin-film transistors (TFTs), where high mobility and on/off ratios are essential. The nascent SWNTs also form as bundles that need to be further dispersed. Numer-